Trajectory tracking for a class of switched nonlinear systems: Application to PMSM[☆]

Lucas N. Egidio[a,b,*], Grace S. Deaecto[a], João P. Hespanha[c], José C. Geromel[d]

[a] *School of Mechanical Engineering, UNICAMP, Campinas, Brazil*
[b] *ICTEAM, Université Catholique de Louvain, Louvain-la-Neuve, Belgium*
[c] *Department of Electrical and Computer Engineering, University of California, Santa Barbara, USA*
[d] *School of Electrical and Computer Engineering, UNICAMP, Campinas, Brazil*

Abstract

This paper proposes a state-dependent switching control for a class of switched nonlinear systems, whose model describes a permanent magnet synchronous machine (PMSM) fed by a three-phase voltage source inverter. Due to its high torque density, high efficiency and wide velocity range, this electrical drive is widely used for traction and several applications in robotics, aerospace, electric vehicles among others. The proposed design conditions are based on a non-quadratic Lyapunov function, dependent on the machine shaft displacement, and assure asymptotic tracking of a pre-specified time-varying rotational velocity profile with guaranteed performance. Properties of the nonlinear system under consideration are used to derive design conditions expressed in terms of linear matrix inequalities that can be solved efficiently. Special cases involving asymptotic stability toward step and ramp velocity profiles are presented. Experimental results are used to validate the proposed technique.

Keywords: Guaranteed cost, Linear matrix inequalities, PMSM, Switched nonlinear systems, Trajectory tracking.

1. Introduction

Permanent magnet synchronous machines (PMSMs), characterized by the presence of permanent magnets in the rotor and a set of windings in the stator, do not require magnetizing currents in the rotor, which enables high torque density, low torque ripple, high efficiency and a wide range of velocities. These characteristics make PMSMs desirable in several high-performance applications such as electrical and hybrid vehicles [1], autonomous water-pumping stations [2], aerospace applications [3], among others. References on modeling and classical control approaches for these machines are available in [4] and [5].

[☆]This research was supported by the "Coordenação de Aperfeiçoamento de Pessoal de Nível Superior (CAPES)", Finance Code 001, by the "National Council for Scientific and Technological Development (CNPq)", under grant numbers 303499/2018-4, and 303887/2014-1, by the São Paulo Research Foundation (FAPESP) under grant number 2017/20343-0 and by the National Science Foundation under grant numbers CNS-1329650 and EPCN-1608880.

[*]Corresponding author : lucas.egidio@uclouvain.be

Email addresses: lucas.egidio@uclouvain.be (Lucas N. Egidio), grace@fem.unicamp.br (Grace S. Deaecto), hespanha@ucsb.edu (João P. Hespanha), geromel@dsce.fee.unicamp.br (José C. Geromel)

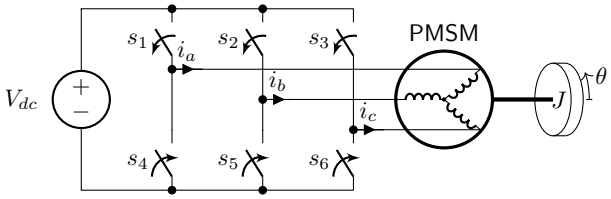

Figure 1: PMSM and inverter schematic

A PMSM is generally fed by a voltage source inverter (VSI) whose switches are operated to command desired voltages to each of the machine phase terminals, see Fig. 1. A standard approach to control these switches, known as field-oriented control (FOC), consists of modeling the machine in terms of an auxiliary rotating reference frame in which the currents are regulated by means of PID controllers together with feedback linearization techniques. Another recurrent approach in the literature is the direct-torque control (DTC), which, in general, controls the machine torque by adopting switching tables that depend on the estimated magnetic flux and torque signals. Nevertheless, both methods require reference frame transformations and a second feedback loop that provides the reference current or torque to the inner loop in order to control the machine shaft velocity or its position. Finally, methodologies based on Model Predictive Control such as [6] have been successful in tackling the control of PMSM but require dealing with online continuous optimization problems. Our goal is to provide an alternative control methodology based on a state-dependent switching rule to decide continuously the state (open or closed) of the VSI switches, bringing the rotor velocity to a desired profile, in a single loop, without using auxiliary reference frames and the associated transformations, and avoiding the solution of continuous or discrete optimization problems at each sampling instant. Insights from switched control theory are leveraged to accomplish this goal.

Switched systems are composed of a set of subsystems, also called operation modes, and a switching function (or switching rule) that selects one of them at each instant of time. Some references on this area include [7], [8] and [9]. For general nonlinear switched systems, some references as [10] provide methods for designing switching functions but these cannot be applied in the case where the subsystems do not share a common equilibrium. Switched affine systems form an important subclass characterized by the presence of affine terms in their dynamic models, allowing for the existence of several equilibrium points, whose stability can be guaranteed by the action of a suitable state or output-dependent switching control. This subclass is used to model a great number of systems in the power electronics domain, see [11], [12] and [13] as representative examples. In the continuous-time domain, design conditions assuring global asymptotic stability of a desired equilibrium point are presented in [14], [12] and [15] while, in the discrete-time domain, stabilizing switching rules are provided in [16] and [17].

The main contribution of this paper is a state-dependent switching control capable of assuring asymptotic tracking to a rotational velocity profile for a PMSM fed by a three-phase VSI. When compared to the previously mentioned switched affine systems, the switching control problem for PMSMs is more challenging due to their dynamic model described by a set of coupled differential equations with sinusoidal functions of the rotor angular displacement. The stability conditions are based on a non-quadratic Lyapunov function that depends on sinusoidal functions of the state variable, whose trigonometric properties are suitably explored to obtain linear matrix inequalities (LMIs). Therefore, the design procedure is cast as a convex optimization problem that minimizes a guaranteed performance cost.

Regarding the state of the art and how this paper improves it, let us comment on some related works available in the literature. The first is a preliminary version of these results dealing solely with asymptotic stability and neglecting friction and external torques, which is available in [18]. In contrast with this preliminary work, the present paper has to deal with the greater difficulty of a trajectory tracking problem, where the rotational angular velocity must follow a time-varying profile whereas the currents converge to appropriate patterns. This represents a more general and intricate problem than the asymptotically stabilization to an equilibrium point tackled in [18]. Also, the assumption that the rotational velocity respects a given upper-bound was replaced by a theoretical guarantee depending on the initial conditions. Another related work is [19], where a switching strategy has been proposed to control PMSMs but based on a quadratic Lyapunov function. However, in this reference the trajectory tracking problem was not formally addressed. In [20] the switching strategy is based on a given control Lyapunov function combined with a backstepping procedure but no systematic methodology to obtain this Lyapunov function is provided. In the present work, we propose a switched controller based on a novel control methodology that provides a smooth transient response when a velocity ramp profile is adopted with guaranteed performance and, when compared to classical FOC methodologies, demands less computational effort and fewer microcontroller peripherals. Simulation and experimental results are provided.

Notation: For real vectors or matrices, $(')$ refers to their transpose. For symmetric matrices, $(\bullet)$ denotes a symmetric block. The identity matrix of appropriate dimension is denoted by I. The symbols $\mathbb{R}$, $\mathbb{R}_+$ and $\mathbb{N}$ denote the sets of real, nonnegative real and natural numbers, respectively. For real and symmetric matrix, $X > 0$ denotes a positive definite matrix. The convex combination of N vectors with the same dimension is denoted as $v_\mu = \sum_{i=1}^{N} \mu_i v_i$ with $\mu \in \Lambda_N$ where $\Lambda_N \subset \mathbb{R}^N$ is the unit simplex, that is, the set of all nonnegative vectors with N components and sum equal to one.

2. Problem Statement

Consider the three-phase permanent magnet synchronous machine with one pair of poles fed by a three-phase inverter with switches $\{s_1, \cdots, s_6\}$ and a DC source V_{dc} depicted in Figure 1. The dynamic model of this assembly is described by the following coupled nonlinear differential equations

$$L\frac{di_a(t)}{dt} + Ri_a(t) = v_a(t) - \lambda\omega(t)f_a(\theta(t)) \tag{1}$$

$$L\frac{di_b(t)}{dt} + Ri_b(t) = v_b(t) - \lambda\omega(t)f_b(\theta(t)) \tag{2}$$

$$L\frac{di_c(t)}{dt} + Ri_c(t) = v_c(t) - \lambda\omega(t)f_c(\theta(t)) \tag{3}$$

together with

$$J\frac{d\omega(t)}{dt} + c\omega(t) = \lambda i_a(t)f_a(\theta(t)) + \lambda i_b(t)f_b(\theta(t)) + \lambda i_c(t)f_c(\theta(t)) - \tau \tag{4}$$

$$\frac{d\theta(t)}{dt} = \omega(t) \tag{5}$$

Table 1: Modes σ, switch states and phase voltages

σ	s_1	s_2	s_3	v_a	v_b	v_c
1	0	0	1	$-V_{dc}/3$	$-V_{dc}/3$	$2V_{dc}/3$
2	0	1	0	$-V_{dc}/3$	$2V_{dc}/3$	$-V_{dc}/3$
3	0	1	1	$-2V_{dc}/3$	$V_{dc}/3$	$V_{dc}/3$
4	1	0	0	$2V_{dc}/3$	$-V_{dc}/3$	$-V_{dc}/3$
5	1	0	1	$V_{dc}/3$	$-2V_{dc}/3$	$V_{dc}/3$
6	1	1	0	$V_{dc}/3$	$V_{dc}/3$	$-2V_{dc}/3$
7	1 0	1 0	1 0	0	0	0

where $i_a(t)$, $i_b(t)$ and $i_c(t)$ are phase currents satisfying $i_a(t) + i_b(t) + i_c(t) = 0$ for all $t \in \mathbb{R}_+$, $v_a(t)$, $v_b(t)$ and $v_c(t)$ are phase to neutral voltages, R and L are the resistance and the equivalent inductance per phase, respectively, J is the rotor moment of inertia, λ is the peak value of the mutual flux linkage, c is the viscous friction coefficient, τ is the external constant torque, $\theta(t)$ is the shaft angular displacement and $\omega(t)$ is the angular velocity. The auxiliary periodic functions $f_a(\theta)$, $f_b(\theta)$ and $f_c(\theta)$ are related to the shape of the back electromotive force (emf) and are defined as

$$f_a(\theta) = \sin(\theta) \tag{6}$$
$$f_b(\theta) = \sin(\theta - 2\pi/3) \tag{7}$$
$$f_c(\theta) = \sin(\theta - 4\pi/3) \tag{8}$$

The voltages $v_a(t)$, $v_b(t)$ and $v_c(t)$ depend exclusively on the state (open or closed) assigned for the switches $\{s_1, \cdots, s_6\}$, at each instant of time. More specifically, s_i is 1 when the switch is closed and 0 when it is open. The control of these switches is the only manner of actuating in the system in order to make the angular velocity $\omega(t)$ asymptotically convergent to a pre-specified profile $\omega^*(t)$ chosen by the designer. Each pair of switches (s_1, s_4), (s_2, s_5), (s_3, s_6) is alternately commanded, i.e., s_1 is closed whenever s_4 is open, and *vice-versa*. Thus, there exist eight possible configurations for the switches, defining seven distinct combinations for the triple $v_a(t)$, $v_b(t)$ and $v_c(t)$ that are represented by the switching function $\sigma \in \mathbb{K} = \{1, \cdots, 7\}$, as detailed in Table 1. This allows us to describe (1)-(5) with the following state space representation

$$\dot{x}(t) = A(\theta(t))x(t) + b_{\sigma(t)},\ x(0) = x_0 \tag{9}$$
$$\dot{\theta}(t) = \omega(t),\ \theta(0) = \theta_0 \tag{10}$$

where $x(t) = [i_\phi(t)'\ \omega(t)]' : \mathbb{R}_+ \to \mathbb{R}^4$ is the state variable with $i_\phi(t) = [i_a(t)\ i_b(t)\ i_c(t)]'$, $\sigma(t) : \mathbb{R}_+ \to \mathbb{K}$ is the switching function to be designed and the matrices $(A(\theta), b_\sigma)$ are given by

$$A(\theta) = \begin{bmatrix} -(R/L)I & -(\lambda/L)f(\theta) \\ (\lambda/J)f(\theta)' & -(c/J) \end{bmatrix},\ b_\sigma = \begin{bmatrix} (1/L)v_\sigma \\ -(\tau/J) \end{bmatrix} \tag{11}$$

where the vector-valued function is $f(\theta) = [f_a(\theta)\ f_b(\theta)\ f_c(\theta)]' : \mathbb{R} \to \mathbb{R}^3$, and the voltage function $v_{\sigma(t)} = [v_a(t)\ v_b(t)\ v_c(t)]' : \mathbb{R}_+ \to \mathbb{R}^3$ takes the values shown in Table 1, for different modes $\sigma(t) \in \mathbb{K},\ \forall t \in \mathbb{R}_+$. In (11), the 3×3 identity matrix is denoted by I.

The main goal of this paper is to design a state dependent function $u(x(t), \theta(t)) : \mathbb{R}^4 \times \mathbb{R} \to \mathbb{K}$ such that the switching control $\sigma(t) = u(x(t), \theta(t))$ guarantees asymptotic tracking to a given

rotational velocity profile $\omega^*(t)$. Ideally the switching function should match the solution to the optimal control problem

$$\min_{\sigma} \int_0^{\infty} \Big(\|(i_\phi(t) - i_\phi^*(t))\|^2 + d^2(\omega(t) - \omega^*(t))^2 \Big) dt \tag{12}$$

where $d > 0$ is a parameter used by the designer to define an appropriate tradeoff between the two components of the total cost and $i_\phi^*(t)$ is the phase current reference vector that is compatible with $\omega^*(t)$ and leads to the least energy dissipation. However, as it has been already discussed in the literature, see for instance [12], this problem is difficult to solve due to the nonlinear nature of the switching control and, therefore, a suboptimal solution is obtained by minimizing a suitable upper bound of (12). In other words, we are particularly interested in assuring the asymptotic convergence of the rotor velocity $\omega(t)$ and phase current vector $i_\phi(t)$ to the desired profiles $\omega^*(t)$ and $i_\phi^*(t)$, respectively.

2.1. Mathematical properties of function $f(\theta)$

The vector-valued function $f(\theta) : \mathbb{R} \to \mathbb{R}^3$ can be written as $f(\theta) = Gg(\theta)$ with

$$G = \begin{bmatrix} 1 & 0 \\ -1/2 & -\sqrt{3}/2 \\ -1/2 & \sqrt{3}/2, \end{bmatrix}, \quad g(\theta) = \begin{bmatrix} \sin(\theta) \\ \cos(\theta) \end{bmatrix} \tag{13}$$

where the matrix $G \in \mathbb{R}^{3\times 2}$ represents the inverse Clarke transformation [21]. Defining the function $D_f(\theta, \omega) = \omega \nabla f(\theta)$ and using (13), simple algebraic manipulations show that, for all $(\theta, \omega) \in \mathbb{R}^2$, the relations

$$\begin{aligned} f(\theta)' f(\theta) &= 3/2 \\ D_f(\theta, \omega)' f(\theta) &= 0 \\ D_f(\theta, \omega)' D_f(\theta, \omega) &= 3\omega^2/2 \end{aligned} \tag{14}$$

hold. Finally, for the unitary vector $e = [1\ 1\ 1]' \in \mathbb{R}^3$ it can be also verified that $e' f(\theta) = 0$ and $e' D_f(\theta, \omega) = 0$. This means that the images of function $f(\theta)$ and of $D_f(\theta, \omega)$ belong to a plane orthogonal to the vector $e \in \mathbb{R}^3$, known as the $\alpha\beta$ plane. We also conclude that, for every scalars $a_1, a_2 \in \mathbb{R}$, the linear combination of $f(\theta)$ and $D_f(\theta, \omega)$ given by $a_1 f(\theta) + a_2 D_f(\theta, \omega)$ always belongs to the circumference

$$\mathbb{F}_\omega = \left\{ y \in \mathbb{R}^3 : e'y = 0,\ \|y\| = \sqrt{3(a_1^2 + a_2^2\omega^2)/2} \right\} \tag{15}$$

For a given $\kappa > 0$, the set $\mathbb{F} = \bigcup_{|\omega| \le \kappa} \mathbb{F}_\omega$ represents an annulus in the $\alpha\beta$ plane with inner and outer radii defined by $\omega = 0$ and $\omega = \pm\kappa$, respectively. The maximal circumference with radius correspondent to $|\omega| = \kappa$ is denoted by $\mathbb{F}_\kappa$.

3. Main Results

Within this section, we present the main results regarding the design of a state dependent switching control capable of assuring asymptotic tracking and minimum guaranteed performance

cost. More specifically, for a given $\kappa \in \mathbb{R}_+$, which defines the velocity domain of interest

$$\Omega_\kappa = \{\omega \in \mathbb{R} \ : \ |\omega| \leq \kappa\} \tag{16}$$

our main goal is to determine a set of attainable rotational velocity profiles $\omega^*(t)$; the associated harmonic currents $i^*_\phi(t) = i^*(t)f(\theta(t))$, where $i^*(t)$ is a scalar valued function; and a switching function $\sigma(t) = u(x(t), \theta(t))$ responsible to orchestrate the state trajectories asymptotically towards $x^*(t) = [i^*_\phi(t)' \ \omega^*(t)]'$ assuring a minimum upper bound for the optimal cost (12). Actually, from a set of initial conditions $(x_0, \theta_0) \in \mathbb{R}^4 \times \mathbb{R}$ and a pre-specified velocity profile $\omega^*(t)$, we need to assure that the rotational velocity $\omega(t)$ does not leave the region (16), i.e., $\omega(t) \in \Omega_\kappa$ for all $t \in \mathbb{R}_+$ and attains the feasible profile $\omega^*(t)$, asymptotically.

To accomplish this goal, consider the auxiliary state variable

$$\xi(t) = x(t) - x^*(t) \tag{17}$$

and the following non-quadratic, radially unbounded (with respect to ξ), Lyapunov function candidate

$$\nu(\xi, \theta) = \xi' P(\theta) \xi \tag{18}$$

where the symmetric matrix valued function $P(\theta) : \mathbb{R} \to \mathbb{R}^{4\times 4}$ is of the form

$$P(\theta) = \begin{bmatrix} pI & \bullet \\ rf(\theta)' & q \end{bmatrix} > 0, \ \forall \theta \in \mathbb{R} \tag{19}$$

The real scalars (p, q, r) are design variables to be determined together with the switching function. Notice that the Lyapunov function (18) is non-quadratic because the matrix $P(\theta)$ is dependent on the state, via the variable $\theta(t)$. This enables us to get a performance guarantee that is much less conservative than with a quadratic function $\nu(\xi) = \xi' P \xi$ that takes a full, but constant, matrix P. We proceed by calculating its time derivative along an arbitrary solution $(\xi(t), \theta(t)), \ \forall t \in \mathbb{R}_+$ of the system under consideration (9)-(10), taking into account that $df(\theta(t))/dt = D_f(\theta(t), \omega(t))$. After some algebraic manipulations we obtain

$$\begin{aligned} \frac{d}{dt}\nu\big(\xi(t), \theta(t)\big) &= \frac{\partial \nu(\xi(t), \theta(t))\big)'}{\partial \xi} \dot{\xi}(t) + \frac{\partial \nu(\xi(t), \theta(t))\big)}{\partial \theta} \dot{\theta}(t) \\ &= -\xi(t)' W\big(\theta(t), \omega(t)\big)\xi(t) + 2\xi(t)' P\big(\theta(t)\big) h_{\sigma(t)}\big(\theta(t), \omega(t)\big) \end{aligned} \tag{20}$$

which holds for all $\xi(t)$ and $\theta(t)$, where the symmetric matrix-valued function $W(\theta, \omega) : \mathbb{R} \times \mathbb{R} \to \mathbb{R}^{4\times 4}$ and the vector-valued function $h_\sigma(t, \theta, \omega) : \mathbb{R} \times \mathbb{R} \times \mathbb{R} \to \mathbb{R}^4$ are

$$W(\theta, \omega) = \begin{bmatrix} 2(Rp/L)I - 2(\lambda r/J) f(\theta) f(\theta)' & \bullet \\ \zeta f(\theta)' - r D_f(\theta, \omega)' & 3\lambda r/L + 2cq/J \end{bmatrix} \tag{21}$$

with $\zeta = Rr/L - \lambda q/J + \lambda p/L + rc/J$ and

$$h_\sigma(t, \theta, \omega) = \begin{bmatrix} v_\sigma/L - \vartheta(t, \theta)/L - i^* D_f(\theta, \omega) \\ (3i^*\lambda/2 - c\omega^* - \tau - J\dot{\omega}^*)/J \end{bmatrix} \tag{22}$$

with $\vartheta(t, \theta) = (Ri^* + \lambda\omega^* + Ldi^*/dt) f(\theta)$. The dependency of h_σ on t occurs through $i^*(t)$, $\omega^*(t)$,

and their derivatives. Notice that, in order to impose the trajectory tracking condition, we need to determine a switching control $\sigma(t) = u(x(t), \theta(t))$ assuring that $d\nu(\xi, \theta)/dt < 0$. Although nontrivial, a solution to this task will be equivalently expressed as an optimization problem described in terms of LMIs and relying on key properties of the nonlinear function $f(\theta)$. The next theorem provides sufficient conditions for the existence of the switching function $u(x, \theta)$, that solves our control design problem. This result assumes that the angular velocity remains within the set defined by (16). We will subsequently provide conditions under which this is guaranteed to hold.

Theorem 1. *Consider the switched nonlinear system (9)-(10) with initial condition (x_0, θ_0). Choose the diagonal matrix $Q = \mathrm{diag}(I, d^2)$ and the scalar $\kappa \in \mathbb{R}_+$ that defines the stability domain of interest Ω_κ given in (16) to which $\omega(t)$ is assumed to belong for all $t \geq 0$. Let the current trajectory $i^*_\phi(t) = i^*(t) f(\theta(t))$ with*

$$i^*(t) = 2\big(c\omega^*(t) + J\dot{\omega}^*(t) + \tau\big)/(3\lambda) \tag{23}$$

where $\omega^*(t)$ is a desired rotational velocity profile such that the signal ω^* belongs to

$$\Omega_* = \Big\{\omega : \Delta(\omega)'\big(\psi\psi' + \kappa^2\varphi\varphi'\big)\Delta(\omega) \leq V_{dc}^2,\ |\omega| \leq \kappa\Big\} \tag{24}$$

where the inequalities in the definition of Ω_* should be understood pointwise in time and

$$\psi = 2/(\sqrt{3}\lambda)\begin{bmatrix} Rc + 3\lambda^2/2 & JR + Lc & JL & R\end{bmatrix}' \tag{25}$$

$$\varphi = 2/(\sqrt{3}\lambda)\begin{bmatrix} Lc & JL & 0 & L\end{bmatrix}' \tag{26}$$

$$\Delta(\omega) = \begin{bmatrix}\omega & \dot{\omega} & \ddot{\omega} & \tau\end{bmatrix}' \tag{27}$$

If there exist scalars (p, q, r) such that $P(\theta) > 0$ and $W(\theta, \omega) > Q$ for all $\theta \in \mathbb{R}$ and $\omega \in \Omega_\kappa$, then the state feedback switching control $\sigma(t) = u(x(t), \theta(t))$ with

$$u(x, \theta) = \arg\min_{j \in \mathbb{K}} \Big([pI \quad rf(\theta)](x - x^*)\Big)' v_j \tag{28}$$

assures that $x(t) \to x^*(t)$ asymptotically. Moreover, the upper bound

$$\int_0^\infty \big(x(t) - x^*(t)\big)' Q \big(x(t) - x^*(t)\big) dt \leq \xi_0' P(\theta_0)\xi_0 \tag{29}$$

for the performance cost (12) holds for all $\xi_0 \in \mathbb{R}^4$.

Proof: To prove asymptotic tracking towards $x^*(t)$, we need to show that for an arbitrary solution of (9)-(10) we have $d\nu(\xi, \theta)/dt < 0$ for all $\xi \neq 0$, $\theta \in \mathbb{R}$ and $\omega \in \Omega_\kappa$. First of all, notice that the choice of the current i^* in (23) makes null the last element of the vector (22). Let us define

$$m(t) = \Big(Ri^* + \lambda\omega^* + L\frac{di^*}{dt}\Big) f(\theta) + Li^* D_f(\theta, \omega) \tag{30}$$

which is a linear combination of $f(\theta)$ and $D_f(\theta, \omega)$ and, as it was discussed earlier, belongs to the set $\mathbb{F}_\omega$ given by (15) with

$$a_1 = Ri^* + \lambda\omega^* + L\frac{di^*}{dt}, \quad a_2 = Li^* \tag{31}$$

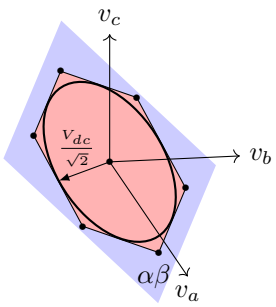

Figure 2: Polytope $\mathbb{P}$ and inscribed circumference $\mathbb{F}_\kappa$

On the other hand, from the values of the phase voltages provided in Table 1, it is a matter of immediate verification that $e'v_j = 0$ for all $j \in \mathbb{K}$ which means that all vectors $v_j,\ j \in \mathbb{K}$, belong to the same $\alpha\beta$ plane in $\mathbb{R}^3$ as $m(t)$ does. The consequence of this important fact that follows from the physical nature of the machine is that at each instant of time $t \in \mathbb{R}_+$ the vector $m(t)$ can be written alternatively as a convex combination of the phase voltages $v_j,\ j \in \mathbb{K}$. More precisely, from these reasonings we can say that while $\omega(t) \in \Omega_\kappa$, there exists $\mu^* \in \Lambda_N$ such that

$$v_{\mu^*} = m(t) \tag{32}$$

if and only if

$$\mathbb{F}_\kappa \subseteq \mathbb{P} = \left\{ v \in \mathbb{R}^3 : v = \sum_{j\in\mathbb{K}} \mu_j v_j,\ \mu \in \Lambda_N \right\} \tag{33}$$

As illustrated in Fig. 2, the circumference of radius $V_{dc}/\sqrt{2}$ is the one of maximum radius inscribed in the polytope $\mathbb{P}$. Thus, taking into account the definition of $\mathbb{F}_\kappa$ just after (15), the inclusion (33) holds if and only if

$$3(a_1^2 + a_2^2\kappa^2)/2 \leq V_{dc}^2/2 \tag{34}$$

for all instants $t \geq 0$ with a_1 and a_2 provided in (31). Substituting the current i^* from (23) into a_1 and a_2 in (31), simple but tedious algebraic manipulations lead to the fact that the inequality (34) holds whenever the desired rotational velocity profile ω^* is chosen inside the set Ω_* defined in (24). That is, the set Ω_* in (24) with the definitions (25)-(27) is obtained directly from (34) after using a_1 and a_2 from (31) with i_* in (23). Now taking into account the existence of $\mu^* \in \Lambda_N$ satisfying (32), the equality (20) together with the switching rule (28) yield

$$\begin{aligned} d\nu(\xi,\theta)/dt &= -\xi' W(\theta,\omega)\xi + \min_{j\in\mathbb{K}} 2\xi' P(\theta) h_j(\theta,\omega) \\ &< -\xi' Q\xi + \min_{\mu\in\Lambda_N} 2\xi' P(\theta) h_\mu(\theta,\omega) \\ &\leq -\xi' Q\xi + 2\xi' P(\theta) h_{\mu^*}(\theta,\omega) \\ &= -\xi' Q\xi \leq 0 \end{aligned} \tag{35}$$

where the first inequality comes from the fact that $W(\theta,\omega) > Q > 0$ and the last equality holds

from the fact that at each instant of time $t \geq 0$ we are able to find $\mu^* \in \Lambda_N$ such that v_{μ^*} satisfies (32), which leads to $h_{\mu^*} = 0$. Hence, $d\nu(\xi,\theta)/dt < 0$ for all $\xi \neq 0$, $\theta \in \mathbb{R}$ and $\omega \in \Omega_\kappa$ implies that $\xi(t) \to 0$ asymptotically. Integrating both sides of (35) from $t = 0$ to $t \to \infty$ we obtain the upper bound (29). The proof is concluded. □

This result provides a switching control that can be applied in the context of trajectory tracking, provided that the desired rotational velocity belongs to the set of feasible trajectories Ω_*, given in (24). Moreover, an upper bound on the associated cost is determined and, as it will be seen next, it can be minimized by an adequate choice of the Lyapunov matrix valued function $P(\theta)$.

An important remark at this point concerns whether Filippov solutions are obtained as a result of the given state-dependent switching law (28). Indeed, these solutions are not ruled out in our methodology but the min-type nature of the switching function still ensures that $x(t) \to x^*(t)$ asymptotically. Consider that at some (ξ,θ) the set of minimizers $\mathcal{I}(\xi,\theta) \subseteq \mathbb{K}$ contains more than one element. For a given $\mu \in \Lambda_{|\mathcal{I}(\xi,\theta)|}$, the time derivative of the Lyapunov function is given by

$$\begin{aligned} d\nu(\xi,\theta)/dt &= -\xi' W(\theta,\omega)\xi + 2\xi' P(\theta) \sum_{i\in\mathcal{I}(\xi,\theta)} \mu_i h_i(\theta,\omega) \\ &= -\xi' W(\theta,\omega)\xi + 2\xi' P(\theta) h_j(\theta,\omega),\ \forall j \in \mathcal{I}(\xi,\theta) \\ &= -\xi' W(\theta,\omega)\xi + \min_{j\in\mathbb{K}} 2\xi' P(\theta) h_j(\theta,\omega) \\ &< 0 \end{aligned} \tag{36}$$

where the first equality comes from the fact that the time derivative $\dot{\xi}(t) = \dot{x}(t) - \dot{x}^*(t)$ follows from the differential inclusion

$$\dot{x}(t) \in \operatorname{co}\{A(\theta(t))x(t) + b_i \ :\ i \in \mathcal{I}(\xi(t),\theta(t))\} \tag{37}$$

see [22] for more details. By definition of $\mathcal{I}(\xi,\theta)$, the second equality follows from the fact that $\xi' P(\theta) h_i(\theta,\omega) = \xi' P(\theta) h_j(\theta,\omega)$ for any $i,j \in \mathcal{I}(\xi,\theta)$, and the last inequality is a consequence of (35). From a practical viewpoint, although real-life switches present physical limitations that prevent Filippov solutions to arise, under high sampling frequencies the behavior of the real system tends to the theoretical one, allowing the implementation of the switching function (28) under a continuous-time perspective. Further discussions on dwell-time constraints and limit behavior is left for future work.

We now turn our attention to the set of initial conditions (ξ_0,θ_0) for which $\omega(t) \in \Omega_\kappa$ for all $t \in \mathbb{R}_+$ and a given $\kappa \in \mathbb{R}_+$, thus satisfying the assumption needed by Theorem 1. The next theorem presents a key result that, together with Theorem 1, assures the tracking property $\omega(t) \to \omega^*(t)$ and $\omega(t) \in \Omega_\kappa$ for any choice of the velocity profile such that $\omega^*(t) \in \Omega_*$ for all $t \in \mathbb{R}_+$.

Theorem 2. *Let a rotational velocity profile $\omega^* \in \Omega_*$, a scalar $\kappa \in \mathbb{R}_+$ and a triple (p,q,r) satisfying the design conditions provided in Theorem 1 be given. Any solution for the system* (9)-(10) *rewritten in terms of ξ as in* (17) *and evolving from $(\xi_0,\theta_0) \in \Xi$ with*

$$\Xi = \left\{(\xi,\theta) \in \mathbb{R}^4 \times \mathbb{R} \ :\ \nu(\xi,\theta) \leq \nu_0\right\} \tag{38}$$

$$\nu_0 = \left(q - \frac{3r^2}{2p}\right) \min_{\varsigma\in\mathbb{R}_+} \left(\kappa - |\omega^*(\varsigma)|\right)^2 \tag{39}$$

satisfies $\omega(t) \in \Omega_\kappa$ *for all* $t \in \mathbb{R}_+$.

Proof: An application of the Schur Complement to (19) shows that $P(\theta) > 0$ for all $\theta \in \mathbb{R}$ if and only if $q > 3r^2/(2p) > 0$. First, considering arbitrary $t \in \mathbb{R}_+$ and $(\xi(t), \theta(t)) \in \Xi$, we have

$$\begin{aligned} \nu_0 &\geq \nu(\xi(t), \theta(t)) \\ &\geq \min_{i_\phi(t) \in \mathbb{R}^3} \nu(\xi(t), \theta(t)) \\ &= \left(q - \frac{3r^2}{2p}\right) \left(\omega(t) - \omega^*(t)\right)^2 \end{aligned} \tag{40}$$

where the equality follows from the application of min operator to (18). This together with (39) yield

$$\begin{aligned} \left(\omega(t) - \omega^*(t)\right)^2 &\leq \min_{\varsigma \in \mathbb{R}_+} \left(\kappa - |\omega^*(\varsigma)|\right)^2 \\ &\leq \left(\kappa - |\omega^*(t)|\right)^2 \end{aligned} \tag{41}$$

Taking into account that $\omega^* \in \Omega_*$ implies $|\omega^*(t)| \leq \kappa$, inequality (41) implies that $-\kappa + |\omega^*| \leq \omega - \omega^* \leq \kappa - |\omega^*|$ from which one concludes that $|\omega(t)| \leq \kappa$ and therefore $\omega(t) \in \Omega_\kappa$. From Theorem 1 it follows that $d\nu(\xi(t), \theta(t))/dt < 0$ whenever $\omega(t) \in \Omega_\kappa$ and we have shown that every $(\xi, \theta) \in \Xi$ is such that $\omega \in \Omega_\kappa$. Since Ξ is a level set of the Lyapunov function, putting all these properties together, we conclude that any trajectory starting in Ξ remains in this set for all $t \in \mathbb{R}_+$, concluding thus the proof. □

It is useful to provide an interpretation of the set Ξ, which is a level set of the Lyapunov function defined by ν_0. Using the fact that

$$\min_{i_\phi(\varsigma) \in \mathbb{R}^3, |\omega(\varsigma)| = \kappa} \nu(\xi(\varsigma), \theta(\varsigma)) = \left(q - \frac{3r^2}{2p}\right)\left(\kappa - |\omega^*(\varsigma)|\right)^2 \tag{42}$$

then it is readily verified that

$$\begin{aligned} \nu_0 &= \min_{\varsigma \in \mathbb{R}_+} \left(q - \frac{3r^2}{2p}\right) \left(\kappa - |\omega^*(\varsigma)|\right)^2 \\ &= \min_{\varsigma \in \mathbb{R}_+} \min_{i_\phi(\varsigma) \in \mathbb{R}^3, |\omega(\varsigma)| = \kappa} \nu(\xi(\varsigma), \theta(\varsigma)) \end{aligned} \tag{43}$$

which indicates that ν_0 defines the largest level set of the Lyapunov function such that $|\omega(\varsigma)| = \kappa$ for all $\varsigma \in \mathbb{R}_+$. Hence, Ξ is the set of initial conditions (ξ_0, θ_0) such that the resulting trajectory respects $\omega(t) \in \Omega_\kappa$ for all $t \geq 0$, fulfilling the assumption needed by Theorem 1.

Additionally, the set of attainable trajectories Ω_* defined in (24) has an especial structure with $\psi\psi'$ and $\varphi\varphi'$ being rank one matrices that allows it to be recast in a different form, reducing the computational cost of verifying whether a given reference ω^* belongs to it. Hence, taking this property into account, Ω_* can be replaced by a simpler although more conservative version

$$\Omega_c = \left\{\omega : \|\Delta(\omega)\|^2 \leq \frac{V_{dc}^2}{\|\psi\|^2 + \kappa^2\|\varphi\|^2},\ |\omega| \leq \kappa\right\} \subseteq \Omega_* \tag{44}$$

which imposes, as expected, a bound on $\Delta(\omega)$ that depends on the physical parameters of the motor and the design parameter $\kappa \in \mathbb{R}_+$.

3.1. Selection of controller parameters

We now devote our attention to the selection of the controller parameters, which include the scalar κ that defines Ω_κ and (p, q, r) that compose the Lyapunov function. The application of this result in each case of interest requires some care as indicated in the sequel. Let us consider the following particular cases that are important in practice:

- **Case 1 :** When the viscous friction coefficient and the external torque can be neglected (e.g. in low-load operations), we can adopt $(c, \tau) = (0, 0)$. This situation has been primarily studied in [18], considering a constant rotational velocity $\omega^*(t) = \omega^*$. It can be noticed that the conditions provided by Theorem 1 are considerably simplified as we only need to take into account scalars $\Delta(\omega) = \omega$, $\psi = \sqrt{3}\lambda$ and $\varphi = 0$ in (24), yielding $\Omega_c \equiv \Omega_* \equiv \Omega_\kappa$ with

$$\kappa = V_{dc}/(\sqrt{3}\lambda) \tag{45}$$

- **Case 2 :** When τ is a non-zero constant, for example corresponding to Coulomb friction, and $\omega^*(t) = \omega^*$ is a desired constant velocity, we can view $\Delta(\omega) = [\omega \ \tau]'$, ψ and φ as vectors in $\mathbb{R}^2$ that follow from the elimination of the second and third elements of (25)-(26). Taking into account that $\psi\psi' + \kappa^2\varphi\varphi' \geq 0$ and that this matrix has all elements non-negative, a necessary and sufficient condition for the convex set Ω_* be equal to Ω_κ follows by imposing that

$$\begin{bmatrix} \kappa \\ |\tau| \end{bmatrix}' \left(\psi\psi' + \kappa^2\varphi\varphi'\right) \begin{bmatrix} \kappa \\ |\tau| \end{bmatrix} \leq V_{dc}^2 \tag{46}$$

  holds for some design parameter $\kappa \in \mathbb{R}_+$. This parameter should be chosen as small as possible to minimize the required value for V_{dc}.

- **Case 3 :** When τ is still constant but the goal is to track a piecewise linear rotational velocity profile ω^*, we need to consider $\Delta(\omega) = [\omega \ \dot{\omega} \ \tau]'$ since $\ddot{\omega}^* = 0$ almost everywhere. This is not an overwhelming restriction as the discontinuous points of ω^* can be considered as new initial conditions for the remaining part of the trajectory. Hence, under this assumption we only need to consider the first, second and fourth elements of (25)-(26). The subset Ω_c given in (44) yields the constraint $\omega^2 + \dot{\omega}^2 \leq \kappa^2$ provided that the 4^{th}-order polynomial inequality

$$\|\varphi\|^2\kappa^4 + \Big(\|\psi\|^2 + \tau^2\|\varphi\|^2\Big)\kappa^2 \leq V_{dc}^2 - \tau^2\|\psi\|^2 \tag{47}$$

  is satisfied for $\kappa \in \mathbb{R}_+$.

Now, an essential requirement of Theorem 1 is to obtain parameters (p, q, r) that satisfy the inequalities $W(\theta, \omega) > Q > 0$ and $P(\theta) > 0$ for all $\theta \in \mathbb{R}$ and $\omega \in \Omega_\kappa$. A computationally intensive approach to this problem would be to exploit the periodicity of $f(\theta)$ by imposing these conditions on a sufficiently fine discrete grid on the box defined by the intervals $|\theta| \leq \pi$ and $|\omega| \leq \kappa$. However, a more efficient manner can be adopted by using the result presented in the next lemma that follows from the properties of the functions $f(\theta)$ and $D_f(\theta, \omega)$.

Lemma 1. *Let the real parameters $(\alpha, \beta, \rho, \eta, \upsilon)$ with $\beta \geq 0$ and $\kappa > 0$ be given. The symmetric matrix-valued function $S(\theta, \omega) : \mathbb{R} \times \mathbb{R} \to \mathbb{R}^{4\times 4}$ defined by*

$$S(\theta,\omega) = \begin{bmatrix} \alpha I - \beta f(\theta) f(\theta)' & \bullet \\ \rho f(\theta)' - \eta D_f(\theta,\omega)' & \upsilon \end{bmatrix} \tag{48}$$

is positive definite for all $\theta \in \mathbb{R}$ and $\omega \in \Omega_\kappa$ if and only if the following conditions

$$2\alpha/3 > \beta,\ 2\upsilon/3 > \left(\frac{\eta^2}{\alpha}\right)\kappa^2 + \left(\frac{\rho^2}{\alpha - 3\beta/2}\right) \tag{49}$$

hold simultaneously.

Proof: Since by assumption $\beta \geq 0$, the first diagonal block of $S(\theta, \omega)$ is positive definite if and only if

$$\begin{bmatrix} \alpha I & \bullet \\ \sqrt{\beta} f(\theta)' & 1 \end{bmatrix} > 0 \tag{50}$$

and the Schur Complement with respect to the first diagonal element indicates that (50) holds if and only if $\alpha > 0$ and $1 > (\beta/\alpha) f(\theta)' f(\theta) = 3\beta/(2\alpha), \forall \theta \in \mathbb{R}$, which is exactly the first condition in (49). Using this fact, the Schur Complement of (48) with respect to the first diagonal element indicates that $W(\theta, \omega) > 0$ if and only if

$$\begin{aligned} \upsilon >& (\rho f(\theta) - \eta D_f(\theta,\omega))' \left(\alpha I - \beta f(\theta) f(\theta)'\right)^{-1} \times \\ & \times (\rho f(\theta) - \eta D_f(\theta,\omega)) \end{aligned} \tag{51}$$

Using the Matrix Inversion Lemma, see [23], it follows that

$$\left(\alpha I - \beta f(\theta) f(\theta)'\right)^{-1} = (1/\alpha) I + (\beta/\alpha)\left(\frac{f(\theta) f(\theta)'}{\alpha - 3\beta/2}\right) \tag{52}$$

which, replaced into (51) and recalling the properties in (14), leads to

$$\begin{aligned} \upsilon &> 3\rho^2/(2\alpha) + 3\eta^2\omega^2/(2\alpha) + (\beta/\alpha)\left(\frac{(3/2)^2\rho^2}{\alpha - 3\beta/2}\right) \\ &= 3\eta^2\omega^2/(2\alpha) + \left(\frac{(3/2)\rho^2}{\alpha - 3\beta/2}\right) \end{aligned} \tag{53}$$

that must be verified for all $\omega \in \Omega_\kappa$. This provides the second inequality in (49) after multiplying both sides by the factor $2/3$, concluding the proof. □

Since the vector-valued function $f(\theta)$ is nonlinear, the result of Lemma 1 is somewhat surprising. Moreover, it is important to notice that the conditions (49) can be equivalently rewritten by means of only one LMI, simplifying the determination of the free parameters involved. The following result shows how to determine the parameters (p, q, r) to minimize the upper bound given in Theorem 1, by solving a convex optimization problem.

Theorem 3. *For given initial conditions (ξ_0, θ_0), matrix $Q > 0$, and $\kappa \in \mathbb{R}_+$, the parameters*

Table 2: Identified system parameters

R	2.19 Ω
L	8.1 $\times 10^{-3}$H
λ	6.0 $\times 10^{-2}$ V.s/rad
c	3.1 $\times 10^{-4}$ N.m.s/rad
J	3.0 $\times 10^{-4}$ kg.m^2
V_{dc}	100 V
τ	8.7 $\times 10^{-3}$ N.m

(p, q, r) solution to the optimization problem

$$\min_{(p,q,r)\in\mathbb{R}^3} \left\{ \xi_0' P(\theta_0)\xi_0 : P(\theta) > 0,\ W(\theta,\omega) - Q > 0, \forall(\theta,\omega) \in \mathbb{R}\times\Omega_\kappa \right\} \tag{54}$$

can be equivalently determined by solving the following convex optimization problem

$$\min_{(p,q,r)\in\mathbb{R}^3} \xi_0' P(\theta_0)\xi_0 \tag{55}$$

subject to

$$\begin{bmatrix} (2/3)q & \bullet \\ r & p \end{bmatrix} > 0 \tag{56}$$

$$\begin{bmatrix} \varrho & \bullet & \bullet \\ \kappa r & (2R/L)p - 1 & \bullet \\ \zeta & 0 & (2R/L)p - (3\lambda/J)r - 1 \end{bmatrix} > 0 \tag{57}$$

with $\varrho = (2\lambda/L)r + (4c/(3J))q - 2d^2/3$ and $\zeta = Rr/L - \lambda q/J + \lambda p/L + rc/J$.

Proof: First, notice that the conditions (49) can be expressed in terms of a linear matrix inequality of the form

$$\begin{bmatrix} 2\upsilon/3 & \bullet & \bullet \\ \kappa\eta & \alpha & \bullet \\ \rho & 0 & \alpha - 3\beta/2 \end{bmatrix} > 0 \tag{58}$$

Now, making $S(\theta,\omega) = P(\theta)$, Lemma 1 assures that inequality (56) is equivalent to $P(\theta) > 0$ for all $\theta \in \mathbb{R}$. In the same manner, writing $S(\theta,\omega) = W(\theta,\omega) - Q$, Lemma 1 assures that inequality (57) is equivalent to $W(\theta,\omega) - Q > 0$ for all $\theta \in \mathbb{R}$ and $\omega \in \Omega_\kappa$. □

The problem (54) always admits a feasible solution (p, q, r) with $q = (J/L)p > 0$, r small enough and $p > 0$ large enough. This means that the design method proposed here always succeeds, provided that the supply voltage V_{dc} is sufficiently large to enable the desired velocity profile ω^*.

4. Simulation and Experimental Results

The previously presented results are ready to be applied to the control of electrical drives, see [5], [24], [25], as some instances. Indeed, trajectory tracking allows us to overcome common practical

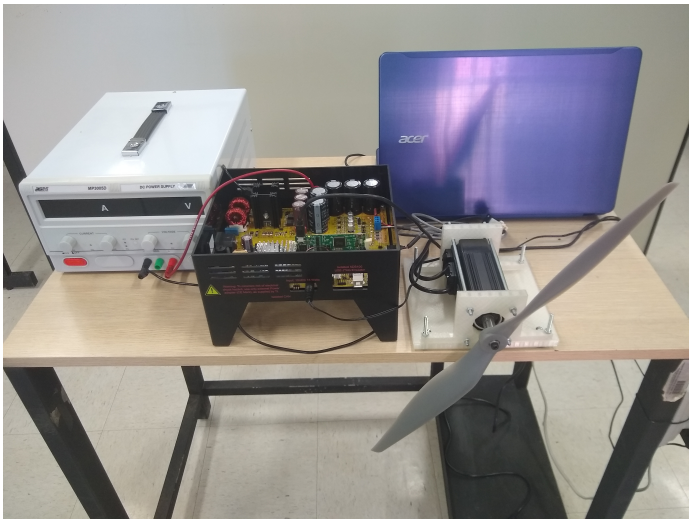

Figure 3: Photo of the experimental setup

issues, e.g. current peaks in transient response, which can be mitigated by adopting adequate reference profiles such as a ramp function as it will be exemplified in this section.

We illustrate our design methodology through the control of a PMSM with parameters in Table 2 fed by a voltage source inverter like the one in Fig. 1. The experimental results were obtained embedding the proposed switching function in a Texas Instruments TMS320F28069 micro-controller (MCU) under sampling frequency $f_s = 40$ kHz. A dead time of 1 μs was considered for operating each pair of switches. Phase currents were measured through shunt resistors and data were acquired by means of built-in analog-to-digital converter and quadrature encoder pulse modules. The motor is the Estun EMJ-04APB24 and a propeller with a diameter of 50.8 cm was attached to its shaft, as shown in Fig. 3. An incremental encoder with 2,500 steps per rotation was used to measure both rotational velocity and displacement. The rotational velocity signal was filtered by means of a first order Butterworth filter with cutoff frequency $\omega_c = 4{,}000$ rad/s, discretized through the bilinear transformation. This allows to calculate the rotational velocity within a suitable precision.

To validate the identified model, we designed the switching function (28) to assure asymptotic convergence of $\omega(t)$ toward a constant $\omega^* = 100$ rad/s. To this end, we selected $\kappa = 314.1593$ rad/s (or 3,000 rpm, the motor rated speed), which assures that $\omega^* \in \Omega_*$. Solving the optimization problem (55) stated in Theorem 3 for $x(0) = 0$, $\theta_0 = 0$, and $Q = \mathrm{diag}(I, 1)$, we obtained the solution

$$p = 2.8790,\ r = 0.0672,\ q = 0.1111 \tag{59}$$

and the upper bound for (29) given by $\xi_0' P(\theta_0)\xi_0 = 1{,}120.23$. For this solution we can calculate $\nu_0 = 4{,}986.07$ from (39), showing that $(\xi_0, \theta_0) \in \Xi$ and, thus, $\omega(t) \in \Omega_\kappa$ for all $t \in \mathbb{R}_+$. For implementation purposes, it is known that real switches cannot operate arbitrarily fast but at high sampling frequencies the real system behavior tends to the nominal one, enabling our strategy to be implemented under a continuous-time perspective.

Figs. 4 and 5 show the closed loop response using the switching function (28) both in simulation and in our hardware test bed. Fig. 6 provides the correspondent experimental switching signal.

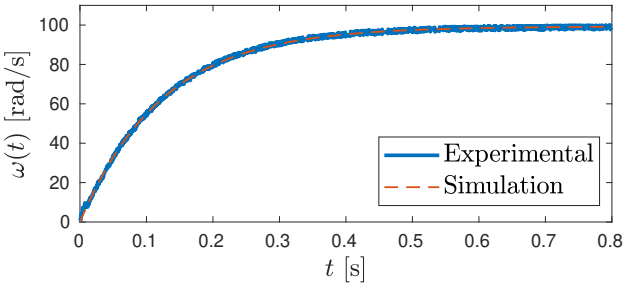

Figure 4: Experimental and simulated velocities for $\omega^* = 100$ rad/s

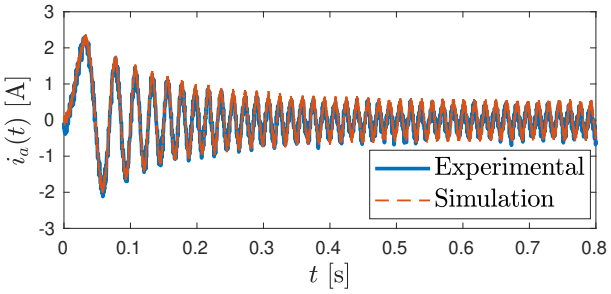

Figure 5: Experimental and simulated phase currents for $\omega^* = 100$ rad/s

The simulated and experimental responses are very close and the angular velocity $\omega(t)$ has attained the desired ω^* as expected, thus validating the proposed control technique as well as the adopted experimental arrangement. For the sake of comparison, solving the analogous problem to (54) but considering a full constant matrix $P > 0$ and imposing $W(\theta) - Q > 0$ over a grid of 100 equally spaced points inside the interval $\theta \in [0, 2\pi]$ leads to an optimal upper bound for (29) given by $\xi_0' P \xi_0 = 4{,}892.92$, about 4 times the one obtained from Theorem 3. This shows how the adopted structure for the Lyapunov function allowed us to obtain less conservative upper bounds for the considered optimal quadratic cost.

As a second experiment, we track a piecewise linear trajectory $\omega^*(t)$ to bring the rotational velocity gradually to 50 rad/s, 100 rad/s and then to a complete stop. This is done by limiting the angular acceleration $|\dot{\omega}(t)| < 50$ rad/s^2, to avoid high peak currents. For the given κ, we have verified that even though discontinuities are present in the time-derivative of the desired velocity profile, $\omega^*(t)$ does belong to the set Ω_* for almost every $t \in \mathbb{R}_+$. Indeed, all the piecewise linear parts of $\omega^*(t)$ belong to Ω_* and, therefore, asymptotic tracking is assured along them. As already mentioned in Case 3, the discontinuities can be viewed as new initial conditions for the remaining state trajectory. Adopting this time-varying reference and the same switching function provided by (59), we obtained the rotational velocity trajectory $\omega(t)$ displayed in Fig. 7 with the desired trajectory $\omega^*(t)$. The associated phase current $i_a(t)$ is displayed in Fig. 8 showing that, by adopting a piecewise linear reference signal, the peak currents have been avoided, obtaining a smoother transient response.

4.1. Computational analysis

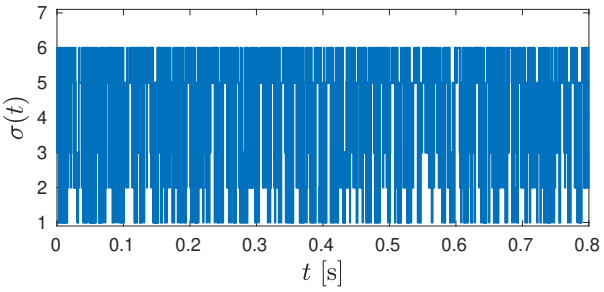

Figure 6: Experimental switching signal for a constant $\omega^* = 100$ rad/s

The proposed switching function (28) can be equivalently replaced by a more efficient one, in terms of required computational effort. In fact, from (28) we have

$$u(x,\theta) = \arg\min_{j\in\mathbb{K}} \Big(pi_\phi + (r\omega - r\omega^* - pi^*)f(\theta)\Big)' v_j \tag{60}$$

$$= \arg\min_{j\in\mathbb{K}} \Big(pGG^{\#}i_\phi + (r\omega - r\omega^* - pi^*)Gg(\theta)\Big)' v_j \tag{61}$$

$$= \arg\min_{j\in\mathbb{K}} \Big(G^{\#}i_\phi + \Big(\frac{r}{p}(\omega - \omega^*) - i^*\Big)g(\theta)\Big)' G' v_j \tag{62}$$

where $G^{\#}$, denoting the Clarke transform, is given by

$$G^{\#} = \frac{2}{3}\begin{bmatrix} 1 & -1/2 & -1/2 \\ 0 & -\sqrt{3}/2 & \sqrt{3}/2 \end{bmatrix} \tag{63}$$

Despite the fact that $GG^{\#} = I - (1/3)ee'$ is not the identity matrix, we always have $GG^{\#}i_\phi = i_\phi$ whenever $i_a + i_b + i_c = 0$. This can be readily shown, since $e'i_\phi = 0$.

Notice that while (60) requires the evaluation of three sine functions and two dot products between vectors in $\mathbb{R}^3$, the expression (62) requires only one sine and one cosine along with two dot products of vectors in $\mathbb{R}^2$, given that $G'v_j$ can be calculated *a priori* for all $j \in \mathbb{K}$. Moreover, observing that the expression inside the min-operator is linear with respect to v_j, it always returns 0 for $v_7 = 0$ and opposite results for the pairs (v_1, v_6), (v_2, v_5) and (v_3, v_4), implying that this expression must be evaluated for only 3 instead of 7 subsystems. Finally, using the fact that $i_c = -i_a - i_b$ we can expand $G^{\#}i_\phi = [i_a \ (-\sqrt{3}/3)(i_a + 2i_b)]'$, simplifying this matrix product to one multiplication and two additions. The division (r/p) and possible scaling factors can also be computed offline.

Implementing the above described strategy, we could perform the calculation of (62) and (23) within 477 clock cycles, using floating-point arithmetic. For the sake of comparison, the field-oriented control approach provided by Texas Instruments ControlSuite needs to compute a Clarke and a Park Transform, three discrete-time PI controller updates, an inverse Park Transform and a Space-Vector generation of PWM signals, which is done within 535 clock cycles also using floating-point arithmetic in the same microprocessor. It is also important to highlight that the use of timer modules for PWM generation is dismissed, which implies less usage of microcontroller peripherals and eventual cost reductions. Notice that these discussions rely on the observations made in

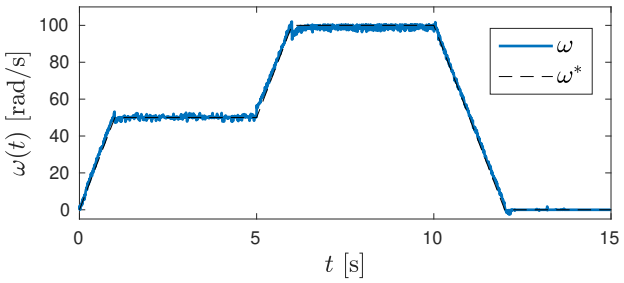

Figure 7: Experimental rotational velocity and reference ω^*

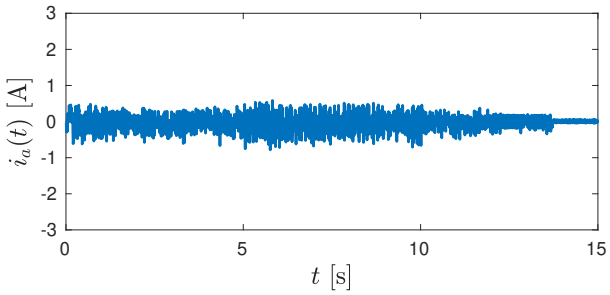

Figure 8: Experimental phase current correspondent to ω^*

the given experimental set-up. Further investigations and other accelerations should be applied, but this preliminary comparison indicates that our approach is implementable and its required computational power is comparable to those of classical control strategies.

5. Conclusions

This paper addresses the design of a state-dependent switching function capable of controlling the switches of a voltage source inverter feeding a permanent magnet synchronous machine, assuring asymptotic tracking to a given rotational velocity profile with a guaranteed performance cost. The design is based on a non-quadratic Lyapunov function and can be equivalently described in terms of LMIs, allowing the use of readily available optimization tools. Experimental results illustrated the efficiency of the proposed design approach and a computational analysis shows that our methodology requires less clock cycles than standard field-oriented control. The study of different electrical drives and several other DC/AC converter applications based on this approach are promising directions for future research. Additionally, problems such as the inclusion of dwell-time, dynamic output feedback, $\mathcal{H}_2$ and $\mathcal{H}_\infty$ performance will be addressed in future works.

References

[1] Z. Yang, F. Shang, I. P. Brown, M. Krishnamurthy, Comparative study of interior permanent magnet, induction, and switched reluctance motor drives for EV and HEV applications, IEEE Transactions on Transportation Electrification 1 (3) (2015) 245–254.

[2] R. Antonello, M. Carraro, A. Costabeber, F. Tinazzi, M. Zigliotto, Energy-efficient autonomous solar water-pumping system for permanent-magnet synchronous motors, IEEE Transactions on Industrial Electronics 64 (1) (2017) 43–51.

[3] T. D. Kefalas, A. G. Kladas, Thermal investigation of permanent-magnet synchronous motor for aerospace applications, IEEE Transactions on Industrial Electronics 61 (8) (2014) 4404–4411.

[4] P. Krause, O. Wasynczuk, S. Sudhoff, S. Pekarek, Analysis of Electric Machinery and Drive Systems, John Wiley & Sons, 2013.

[5] R. Krishnan, Permanent Magnet Synchronous and Brushless DC Motor Drives, CRC press, 2009.

[6] J. Rodriguez, P. Cortes, Predictive control of permanent magnet synchronous motors.

[7] R. A. DeCarlo, M. S. Branicky, S. Pettersson, B. Lennartson, Perspectives and results on the stability and stabilizability of hybrid systems, Proceedings of the IEEE 88 (7) (2000) 1069–1082.

[8] D. Liberzon, Switching in Systems and Control, Birkhauser, 2003.

[9] Z. Sun, S. S. Ge, Stability theory of switched dynamical systems, Springer Science & Business Media, 2011.

[10] Q. Liu, L. Long, State-dependent switching law design with guaranteed dwell time for switched nonlinear systems, International Journal of Robust and Nonlinear Control 30 (8) (2020) 3314–3331.

[11] G. Beneux, P. Riedinger, J. Daafouz, L. Grimaud, Adaptive stabilization of switched affine systems with unknown equilibrium points: Application to power converters, Automatica 99 (2019) 82–91.

[12] G. S. Deaecto, J. C. Geromel, F. Garcia, J. Pomilio, Switched affine systems control design with application to dc–dc converters, IET Control Theory & Applications 4 (7) (2010) 1201–1210.

[13] L. N. Egidio, H. R. Daiha, G. S. Deaecto, J. C. Geromel, DC motor speed control via buck-boost converter through a state dependent limited frequency switching rule, in: Conference on Decision and Control (CDC), 2017, pp. 2072–2077.

[14] P. Bolzern, W. Spinelli, Quadratic stabilization of a switched affine system about a nonequilibrium point, in: American Control Conference, Vol. 5, 2004, pp. 3890–3895.

[15] A. Trofino, D. Assmann, C. C. Scharlau, D. F. Coutinho, Switching rule design for switched dynamic systems with affine vector fields, IEEE Transactions on Automatic Control 54 (9) (2009) 2215–2222.

[16] G. S. Deaecto, J. C. Geromel, Stability analysis and control design of discrete-time switched affine systems, IEEE Transactions on Automatic Control 62 (8) (2017) 4058–4065.

[17] L. N. Egidio, H. R. Daiha, G. S. Deaecto, Global asymptotic stability of limit cycle and $\mathcal{H}_2/\mathcal{H}_\infty$ performance of discrete-time switched affine systems, Automatica 116 (2020) 108927.

[18] L. N. Egidio, G. S. Deaecto, J. P. Hespanha, J. C. Geromel, A nonlinear switched control strategy for permanent magnet synchronous machines, in: Conference on Decision and Control (CDC), 2019, pp. 3411–3416.

[19] R. Delpoux, L. Hetel, A. Kruszewski, Parameter-dependent relay control: Application to PMSM, IEEE Transactions on Control Systems Technology 23 (4) (2014) 1628–1637.

[20] G. Prior, M. Krstic, Quantized-input control Lyapunov approach for permanent magnet synchronous motor drives, IEEE Transactions on Control Systems Technology 21 (5) (2012) 1784–1794.

[21] W. C. Duesterhoeft, M. W. Schulz, E. Clarke, Determination of instantaneous currents and voltages by means of alpha, beta, and zero components, Transactions of the American Institute of Electrical Engineers 70 (2) (1951) 1248–1255.

[22] A. F. Filippov, Differential Equations with Discontinuous Right-Hand Side, Kluwer Academic Publisher, 1988.

[23] R. A. Horn, C. R. Johnson, Matrix Analysis, Cambridge University Press, 1990.

[24] N. Matsui, M. Shigyo, Brushless dc motor control without position and speed sensors, IEEE Transactions on Industry Applications 28 (1) (1992) 120–127.

[25] P. Pillay, R. Krishnan, Modeling, simulation, and analysis of permanent-magnet motor drives. I. The permanent-magnet synchronous motor drive, IEEE Transactions on Industry Applications 25 (2) (1989) 265–273.